

# Protein Electron Transfer Reorganization Energy Spectrum from Normal Mode Analysis. 1. Theory

Gautam Basu,<sup>\*,†</sup> Akio Kitao,<sup>‡</sup> Atsuo Kuki,<sup>§</sup> and Nobuhiro Go<sup>\*,‡</sup>

Department of Biophysics, Bose Institute, P-1/12 CIT Scheme VIIM, Calcutta 700054, India, Department of Chemistry, Graduate School of Science, Kyoto University, Kyoto 606-8502, Japan, and Alanex Corporation, 3550 General Atomics Court, San Diego, California 92121

Received: September 2, 1997; In Final Form: January 6, 1998

We present an analytical model that describes the coupling of protein fluctuations to electron transfer. The model treats both the protein and the bulk solvent to couple to electron transfer. The protein is represented by a low-dielectric cavity containing explicit protein atoms, and the bulk solvent is represented by a high-dielectric continuum surrounding the cavity. Protein fluctuations are modeled by collective normal modes with solvation energies incorporated through explicit reaction field energies. The shifts of the equilibrium normal mode variables upon electron transfer, related to the mode-specific couplings and reorganization energies, are calculated assuming the difference of the potential energy surfaces before and after electron transfer by a hyper plane in the normal mode vector space. This linear coupling assumption allows only one set of normal mode vectors to span both the reactant and product equilibrium conformations. The model is equivalent to a reduced spin–boson formalism (protein only); however, unlike previous work within this formalism, the bath modes are not spatially anonymous in our treatment. They are associated with unambiguous frequency and spatial signatures allowing a spectral analysis of protein reorganization energy with one-to-one connection with actual protein fluctuation. This aspect of our model is very crucial since it allows, for the first time, to make a direct connection between actual protein motion and electron transfer, as demonstrated by a simulation presented in an accompanying paper (*J. Phys. Chem.* **1998**, 102, XXX).

## 1. Introduction

Electron transfer (ET) is one of the most fundamental processes in chemistry and biology, and accordingly it has attracted significant attention from researchers in diverse disciplines in recent years. In biological systems, there are several classes and types of proteins that mediate ET,<sup>1</sup> all probably optimized via evolution for a specific purpose. To understand how these proteins work, or how protein-mediated ET differs from one that is not protein-mediated, a sound understanding of the theoretical aspects of the process is needed, especially one that can pinpoint protein involvement in the reaction at atomic resolution. Besides, such an understanding will also provide insights into designing artificial systems that can act as energy transducers, including those that harness solar energy.

Theoretical aspects of nonadiabatic ET process are well-established within the classical, semiclassical, and quantum mechanical framework.<sup>2–8</sup> In all these theories the first step is a partition of the ET rate constant  $k_{\text{ET}}$  into two factors: the electronic factor  $H_{\text{DA}}$  and the nuclear factor FC.

$$k_{\text{ET}} = \left(\frac{2\pi}{\hbar}\right) H_{\text{DA}}^2 \text{FC} \quad (1)$$

The factor  $H_{\text{DA}}$  contains information about the total (direct and indirect) interaction of the donor–acceptor electronic wave functions. A major protein contribution to  $H_{\text{DA}}$  arises through enhancing the indirect interaction of the donor–acceptor

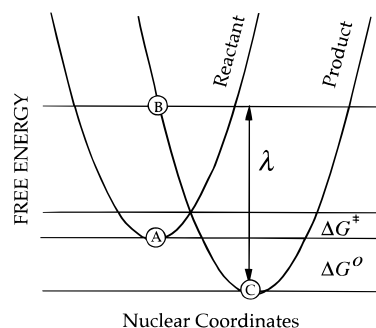


**Figure 1.** Free energy curves before and after electron transfer as a function of nuclear coordinates of the system.

electronic wave functions.<sup>9</sup> The three-dimensional skeleton of the protein further restricts the distance and orientation of the donor–acceptor sites, thereby affecting  $H_{\text{DA}}$ .

The factor FC is related to the fluctuations and relaxation of the nuclear polarization of the medium. In classical treatment of ET, a key parameter in the FC factor is the reorganization energy,  $\lambda$ , defined as the free energy change associated with the relaxation of the entire set of nuclear coordinates surrounding the red-ox sites as the charge distribution changes from the reactant (R) to the product (P) state. In Figure 1 this is shown as the free energy released as the nonequilibrium state B relaxes to the equilibrium state C. The FC factor, with explicit  $\lambda$  dependence, is given by

$$\text{FC} = \frac{1}{\sqrt{4\pi\lambda k_{\text{B}}T}} \exp\left\{-\frac{(\Delta G^{\circ} + \lambda)^2}{4\lambda k_{\text{B}}T}\right\} \quad (2)$$

<sup>†</sup> Bose Institute.

<sup>‡</sup> Kyoto University.

<sup>§</sup> Alanex Corp.

The involvement of the protein matrix in FC, like in the case of  $H_{DA}$ , is also direct and indirect. Indirectly, by keeping the polarizable solvent (usually water) away from the immediate vicinity of the red-ox sites, it can make FC less solvent-dependent. Concomitantly, by actually surrounding the red-ox sites, the protein affects the FC factor via the coupling of protein nuclear polarization fluctuations with the change of electronic state during ET, the electron–conformation ( $e$ – $c$ ) coupling.

In recent years a number of studies have attempted to address the question of  $e$ – $c$  coupling by molecular dynamics (MD) simulation and subsequent analysis of the trajectory.<sup>10–16</sup> The key microscopic variable of interest in these studies is the energy difference between the R and the P states.<sup>17</sup> Probability distributions of this energy difference and its autocorrelation function serve as the starting point for a quantitative analysis of the  $e$ – $c$  coupling. These approaches are suitable for assessing the total coupling of the entire nuclear degrees of freedom. For ET in proteins, the total coupling arises from the degrees of freedom of the protein as well as from the bulk solvent. In terms of spatial identities of conformational fluctuations that couple to ET, it is the protein fluctuations that are of prime interest. In this regard it is important that a formal breakup of the total coupling be made among the protein and the bulk material, as was attempted earlier.<sup>18</sup> In addition, a model that can break down the protein coupling into a spectrum spanning the entire conformational space of the protein atoms is desirable. In this paper we present a model that resolves the protein coupling into such a spectrum.

Typically a protein molecule is very large, with its tertiary structure governed dominantly by weak nonbonded interactions. This gives rise to several low-frequency collective breathing modes which arise due to sampling of the soft dihedral angle space.<sup>19,20</sup> In the case of large macromolecules such as proteins, a natural question is whether soft collective modes contribute importantly to the coupling. There are other important issues as well. Since the protein matrix is a highly heterogeneous medium, the variation of  $k_{ET}$ , as a function of red-ox pair distance and disposition within the protein matrix, is quite complex. Theoretical understanding has typically been sought through modeling the  $H_{DA}$  term.<sup>9,21,22</sup> But what if changes in the distance and disposition of the red-ox sites or mutations in the medium also affect the soft (or, for that matter, hard) modes whose contribution to FC is large? To have a comprehensive understanding of all of these issues, it is extremely important that a theoretical framework be developed that allows one to explicitly calculate the mode-specific contributions of  $e$ – $c$  coupling in proteins.

In the past, the medium surrounding the red-ox sites has been treated as a uniform continuum,<sup>4,5</sup> as a piecewise constant dielectric continuum,<sup>23</sup> or as a set of quantum harmonic oscillators (inner sphere formula<sup>3</sup>). In this paper we use a new approach, where we carry out the natural generalization of the inner sphere treatment to the more complex “oscillator” of the atomistic model of a protein contained in a cavity surrounded by a continuum dielectric (Figure 2).

Fluctuations of this atomistic protein molecule, contained in a low-dielectric cavity and surrounded by a higher dielectric continuum, are modeled by collective normal modes (NM) around a minimum energy conformation (MEC). It is the collective nature of these modes that becomes crucial in the theory. The mode-specific couplings are related to the mode-specific shift of the MEC upon ET. Bulk solvent contribution to the ET is incorporated through two separate effects. The primary effect of the bulk solvent arises from the relaxation of

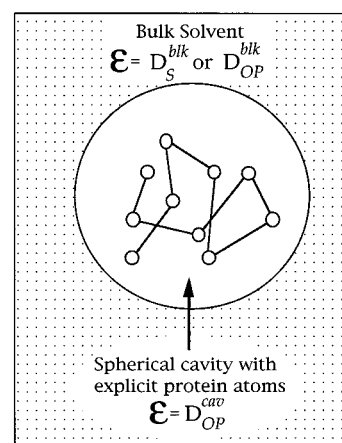


**Figure 2.** Schematic description of the protein–solvent system. The bulk solvent is represented by a continuum dielectric with dielectric constant of  $D_{OP}^{blk}$  or  $D_S^{blk}$ , and the atomistic protein is considered to lie within a spherical cavity with dielectric constant  $D_{OP}^{cav}$ . Of the total number of protein atoms, charges ( $q_i$ ) on  $N$  atoms do not change upon ET, while the other  $M$  sites change charge on ET ( $Q_i$  to  $Q_i + \Delta Q_i$ ).

the solvent nuclear polarization upon ET. The other and more subtle effect is the equilibrium solvation energy of the protein. While the former effect gives rise to a single reorganization parameter, the latter effect is resolved along all the protein collective modes through reaction field energies.

This is the first attempt that quantifies the coupling of atomistic collective modes to ET retaining full spatial signatures of the modes. Our model is analytic and provides important physical insight into the problem including a redefinition of the inner sphere and outer sphere contributions to reorganization energy. The strength of this model lies in the fact that it is not just phenomenological but can be accessed by molecular simulations. In a following paper we demonstrate the applicability of this model by a simulation on Ru-modified cytochrome *c*.<sup>24</sup>

## 2. Formulation of the Problem

**2.1. Description of the System.** Before elaborating on the theoretical aspects of ET and its coupling to nuclear fluctuations, we first describe the protein–solvent system, as treated in this paper. The protein molecule is represented by explicit atoms whose fluctuations are modeled by normal mode analysis (NMA). The protein molecule is composed of  $(M + N)$  atoms; charges on  $M$  sites change with ET (denoted by  $Q_i$  and  $Q_i + \Delta Q_i$ ), while charges on  $N$  sites do not change with ET (denoted by  $q_i$ ). This atomistic protein is placed inside a spherical dielectric cavity representing the protein shape. The spherical cavity is surrounded by a structureless continuum dielectric representing the bulk solvent. A schematic description of the system is shown in Figure 2. The choice of the dielectric constants used for the cavity and the bulk solvent, as indicated in Figure 2, is justified in section 2.2. The primary motivation for choosing this special model (piecewise continuous and atomistic) is to represent the electrostatic interactions, responsible for coupling of nuclear modes to ET, as realistically as possible together with the requirement that several energy evaluations can be performed within a reasonable amount of time.

Protein conformational fluctuations are modeled, as described above, by normal mode analysis in the following formulation. Normal mode analysis is based on the assumption that the conformational energy function is harmonic within the range

of thermal fluctuations. However, it is already known that this assumption does not hold precisely for proteins. Even so, it is also known that, as far as second moments of fluctuations of atomic positions are concerned, normal mode analysis can be extended as principal component analysis<sup>25,26</sup> to take into account of effects of anharmonicities. Even though the following formulation is developed in terms of normal mode analysis, most of the resulting formulas can be reinterpreted as valid also for principal component analysis. Therefore, the formulation developed in the following is in fact effective even when conformational fluctuations are highly anharmonic.

The simple Coulomb's law with a uniform dielectric constant poorly models electrostatic interactions of heterogeneous systems. Especially for large low-dielectric molecules such as proteins, this simple expression utterly fails to represent two salient and important features in the actual electrostatic energy. The self-energies of the atoms, arising from the polarization effect of the solvent, are completely ignored. These self-terms are primarily responsible in accounting for the solvation energy. Also, the screening of the pairwise energies due to polarization terms is very poorly represented by the uniform or a distance-dependent dielectric constant. There are two methods currently available to partly overcome these deficiencies. One can either use the microscopic PDL approach developed by Warshel and Levitt<sup>27,28</sup> or use a macroscopic piecewise continuous dielectric model based on solving the Poisson–Boltzmann (PB) equation made popular partially due to the work by Honig and co-workers.<sup>29</sup> Because of its simplicity and capability to perform calculations on large systems, we employ the latter method for this work.

The parent equation for continuum dielectric models is the PB equation

$$\nabla \cdot [\epsilon(\mathbf{r}) \cdot \nabla \Omega(\mathbf{r})] - \bar{\kappa}_0^2 \Omega(\mathbf{r}) - 4\pi\rho(\mathbf{r}) = 0 \quad (3)$$

where  $\Omega(\mathbf{r})$  is the electrostatic potential,  $\rho(\mathbf{r})$  is the free charge density,  $\epsilon(\mathbf{r})$  is the spatially variant dielectric constant, and  $\bar{\kappa}_0^2$  is related to ionic strength effects. The simplest approach to model the function  $\epsilon(\mathbf{r})$  is to consider the protein to be a low-dielectric cavity immersed in a high-dielectric bulk solvent. For a realistic protein (cavity) shape, eq 3 cannot be solved analytically due to complicated boundary conditions.

Instead, numerical solutions to eq 3 can be obtained, typically calculated only for a single static conformation. In our model, we need to perform energy minimization of the protein molecule, and that requires several thousand steps of energy and gradient evaluations. A spherical boundary for the protein is the next practical solution since the solution to eq 3 under this boundary condition becomes analytical. Expressions for the spherical cavity model were first derived by Kirkwood<sup>30</sup> and later applied to proteins by Tanford and Kirkwood (TK).<sup>31</sup> We will neglect all ionic strength effects in this work. The total electrostatic energy is the sum of all atomic pair terms ( $i \neq j$ ) and the self-reaction-field term ( $B_{ii}$ ). Direct Coulombic self-terms ( $A_{ii}$ ) are absent. Thus it is given by

$$\begin{aligned} E_{\text{electro}} &= \frac{1}{2b} \sum_{i,j} e_i e_j (A_{ij} - B_{ij}) \\ &= \frac{1}{b} \sum_{i>j} e_i e_j (A_{ij} - B_{ij}) - \frac{1}{2b} \sum_i e_i^2 B_{ii} \end{aligned} \quad (4)$$

where  $b$  and  $a$  are the cavity and the ion-exclusion radii, respectively, and  $e_i$  is the charge on the  $i$ th site; the term  $A_{ij}$

represents the direct Coulomb interactions; the term  $B_{ij}$  represents the reaction field effect from the solvent. The sum of  $B_{ij}$  and  $A_{ij}$  terms will later be written as  $E_{\text{RF}}$ . Full expressions for the  $A_{ij}$  and the  $B_{ij}$  terms are given by

$$\begin{aligned} A_{ij} &= \frac{b}{D_{\text{in}} r_{ij}} \\ B_{ij} &= \frac{1}{D_{\text{in}}^{n+1}} \sum_{n=0}^{\infty} \frac{(n+1)(D_{\text{out}} - D_{\text{in}})}{(n+1)D_{\text{out}} + nD_{\text{in}}} \left( \frac{r_i r_j}{b^2} \right)^n P_n(\cos \theta_{ij}) \end{aligned} \quad (5)$$

where  $b$  is the radius of the cavity,  $r_i$  and  $r_j$  are the radial distances of atom  $i$  and  $j$  with charges  $e_i$  and  $e_j$ ,  $\cos \theta_{ij}$  is the cosine of the angle between  $\vec{r}_i$  and  $\vec{r}_j$ , and  $P_n(\cos \theta_{ij})$  are the Legendre polynomials of order  $n$ .

**2.2. Nuclear Relaxations upon ET.** The response of the nuclear coordinates surrounding the red-ox sites that couple to ET is exhibited by a characteristic relaxation to a new equilibrium configuration upon ET. Since the only change that the ET process brings about is a change in the charge distribution at the red-ox sites, this relaxation occurs solely due to the corresponding change in the electric field permeating the medium. There are two separate origins for this relaxation: (1) redistribution of the electron density around the medium nuclei, represented by the change in the electronic polarization  $P_e$ , and (2) reorientation of the permanent dipoles and mobile ions in the medium, represented by the change in the nuclear polarization  $P_n$ . Because of the time scales involved, it is assumed that the electronic polarization  $P_e$  relaxes instantaneously with ET, while the nuclear polarization  $P_n$  lags behind.

In continuum electrostatic models, the effect of the equilibrium medium polarizations is modeled through the dielectric constant, where the high-frequency (optical) dielectric constant represents the effect of only  $P_e$ , while the zero-frequency (static) dielectric constant represents the effects from both  $P_e$  and  $P_n$ . Marcus, in his original work on classical theory of ET, had derived an expression for the nonequilibrium (with respect to the product red-ox site charge distribution) polarization  $P_n$  produced upon ET. This is the key equation that led Marcus<sup>4,5</sup> to write expressions for  $\lambda$  as a function of both the optical and the static dielectric constants.

One of the goals of this paper is to derive suitable  $\lambda$  expressions for the entire system, as separate contributions from the protein and the bulk solvent. We treat the bulk solvent as a structureless continuum, and as a consequence, the treatment of the bulk contribution to  $\lambda$  is similar to that of Marcus. Expressions for  $\lambda^{\text{blk}}$ , as elaborated later, accordingly call for the use of the static ( $D_S^{\text{blk}}$ ) as well as the optical ( $D_{\text{OP}}^{\text{blk}}$ ) dielectric constants of the bulk solvent, as indicated in Figure 2. In contrast, we treat the fluctuations of the permanent dipoles of the atomistic protein explicitly by classical simulation methods, and so the protein cavity is characterized by only the optical dielectric constant ( $D_{\text{OP}}^{\text{cav}}$ ) of the cavity, also indicated in Figure 2.

**2.3. Protein and Bulk Solvent Contributions.** The ET process is accompanied by the relaxation of the entire collection of nuclear coordinates that surround the red-ox sites. Since the protein coordinates, due to bonding and other constraints, are much more restricted to relax than the bulk solvent coordinates, it is natural that the two relaxations be treated separately. Further, it is the protein relaxations whose structural signatures have relevance to design and control of ET through special protein architectures.

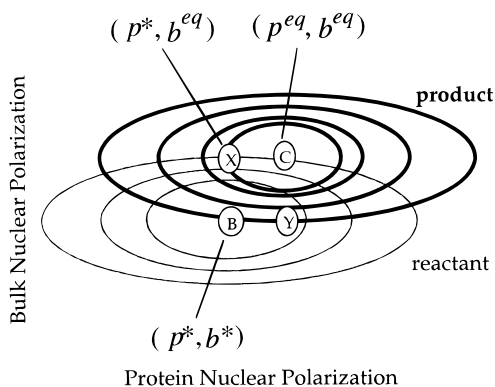


**Figure 3.** Free energy surfaces of reactant (thin line) and product (thick line) states along the protein and bulk nuclear polarization. Points B, X, C, and Y lie on the product energy surface.

One way to represent independent relaxations of the bulk solvent and protein nuclear coordinates is to redraw Figure 1 as Figure 3, where, instead of free energy *curves* along only a single nuclear coordinate (bulk solvent plus protein), free energy *surfaces* are shown as contour plots along the bulk (*b*) and the protein (*p*) nuclear coordinates. The relevant nuclear coordinates in ET can be represented by the corresponding nuclear polarizations. The points B, C, X, and Y, shown in Figure 3, lie on the product-state free energy surface; superscripts eq and \* indicate equilibrium and nonequilibrium polarizations with respect to the final-state charge distribution. Points B and C correspond to B and C in Figure 1. Two new points, Y and X, have been labeled in Figure 3; at Y the protein polarization is in equilibrium ( $p^{eq}, b^*$ ), whereas at X the bulk polarization is in equilibrium ( $p^*, b^{eq}$ ). According to Figure 3 the total reorganization energy can be formally broken down as

$$\lambda\{p^*, b^* \rightarrow p^{eq}, b^{eq}\} = \lambda^{blk}\{p^*, b^* \rightarrow p^*, b^{eq}\} + \lambda^{prot}\{p^*, b^{eq} \rightarrow p^{eq}, b^{eq}\} \quad (6)$$

In the next section we derive appropriate expressions for the bulk solvent contribution to total  $\lambda$ ,  $\lambda^{blk}$ .

### 3. Bulk Solvent Relaxation: $\lambda^{blk}$

To estimate  $\lambda^{blk}\{p^*, b^* \rightarrow p^*, b^{eq}\}$ , one requires a knowledge of the nonequilibrium states ( $p^*, b^*$ ) and ( $p^*, b^{eq}$ ). Although the polarizations  $p^*$  and  $b^*$  are in equilibrium with respect to the reactant charge distribution, they are nonequilibrium polarizations with respect to the new product charge distribution. In this respect, they represent “special” nonequilibrium states, and Marcus’s original work<sup>4,5</sup> exploited this fact. While Marcus’s canonical expression for the reorganization energy was derived for two conducting spheres in a dielectric continuum, later a similar approach was used to derive  $\lambda$  expressions for other geometries as well.<sup>23</sup>

Let us consider the system described in Figure 2, where the electrostatic energy is given by eq 4. We want to write the energy difference between points B and X in Figure 3 as  $\lambda^{blk}$ . A convenient thermodynamic cycle for achieving this is the following

$$\lambda^{blk} = W_{X \rightarrow B} = W_{X \rightarrow A} + W_{A \rightarrow B} \quad (7)$$

where  $W$  represents the reversible work done for processes indicated in the subscripts; A is a state on the reactant free energy surface immediately below the state B and is therefore characterized by nuclear polarization ( $p^*, b^*$ ). The electrostatic

potential for the three states can be written as<sup>23</sup>

$$\psi^B(\mathbf{r}_i) = \left\{ \sum_j e_j^R F_{ij}(D_S^{blk}) - \sum_j e_j^R F_{ij}(D_{OP}^{blk}) \right\} + \sum_j e_j^P F_{ij}(D_{OP}^{blk}) \quad (8)$$

$$\psi^X(\mathbf{r}_i) = \left\{ \sum_j e_j^P F_{ij}(D_S^{blk}) - \sum_j e_j^P F_{ij}(D_{OP}^{blk}) \right\} + \sum_j e_j^P F_{ij}(D_{OP}^{blk}) \quad (9)$$

$$\psi^A(\mathbf{r}_i) = \left\{ \sum_j e_j^R F_{ij}(D_S^{blk}) - \sum_j e_j^R F_{ij}(D_{OP}^{blk}) \right\} + \sum_j e_j^R F_{ij}(D_{OP}^{blk}) \quad (10)$$

where  $e_j^R$  and  $e_j^P$  are the reactant and product charge distributions respectively,  $F_{ij}$  is equal to  $(A_{ij} - B_{ij})/b$  in eq 4, and the dependence of  $F_{ij}$  on  $D_{OP}^{cav}$  is implicit. Since the protein nuclear polarization in all three states, A, B, and X, are all  $p^*$ , the dependence of  $F_{ij}$  on the equilibrium atomic coordinates in the R state  $\mathbf{r}_{eq}^R$  is also implicitly assumed. Expressions for the reversible work can be written as<sup>23</sup>

$$W_{X \rightarrow A} = \frac{1}{2} \sum_{ij} e_i^R e_j^R F_{ij}(D_S^{blk}) - \frac{1}{2} \sum_{ij} e_i^P e_j^P F_{ij}(D_S^{blk}) \quad (11)$$

$$W_{A \rightarrow B} = \sum_{ij} e_i^P e_j^R F_{ij}(D_S^{blk}) - \sum_{ij} e_i^P e_j^R F_{ij}(D_{OP}^{blk}) + \frac{1}{2} \sum_{ij} e_i^P e_j^P F_{ij}(D_{OP}^{blk}) - \sum_{ij} e_i^R e_j^R F_{ij}(D_S^{blk}) + \sum_{ij} e_i^R e_j^R F_{ij}(D_{OP}^{blk}) - \frac{1}{2} \sum_{ij} e_i^R e_j^R F_{ij}(D_{OP}^{blk}) \quad (12)$$

Using eqs 7, 11, and 12, the final expression for  $\lambda^{blk}$  becomes

$$\lambda^{blk} = \frac{1}{2} \sum_{ij} [(e_i^P - e_i^R)(e_j^P - e_j^R)\{F_{ij}(D_{OP}^{blk}) - F_{ij}(D_S^{blk})\}] \quad (13)$$

This can also be rewritten as

$$\lambda^{blk} = E_{RF}(\Delta Q_i, D_{OP}^{prot}, D_{OP}^{blk}) - E_{RF}(\Delta Q_i, D_{OP}^{prot}, D_S^{blk}) \quad (14)$$

### 4. Protein Relaxation: $\lambda^{prot}$

In the previous section we derived expressions for the bulk solvent contribution to  $\lambda$  (eq 14). In this section we derive the protein contribution to  $\lambda$ ,  $\lambda^{prot}$ . Unlike the bulk solvent, the nuclear fluctuations of the protein are treated explicitly through NMA (section 4.1). Each NM is associated with a mode-specific  $\lambda^{prot}$ ,  $\lambda_k^{prot}$ , collectively making up the protein reorganization spectrum, as described in section 4.2. In section 4.3 we outline the relationship between the R and the P state energies, used later to derive analytical expressions for  $\lambda_k^{prot}$  with TK reaction field energies (section 4.4). To emphasize the spectral analysis through NMA  $\{\lambda_k^{prot}\}$ , we call it the normal mode reorganization energy spectrum (NMRES) model. The NMRES model is compared with other linear models in section 4.5, where distinguishing features of our approach are pointed out. In section 4.6, as a natural followup of the NMRES model, new ways to partition  $\lambda$  are proposed.

**4.1. Collective Mode Description of Protein Motion through Normal Modes.** The classical Hamiltonian that determines the energy of a molecular conformation or that dictates the time dependence of the molecule in the multidimensional

mensional conformational space is quite complex. This Hamiltonian can be represented by an empirical energy function  $E$ , which is given by

$$E = \sum_{\text{bonds}} K_r(r - r_{\text{eq}})^2 + \sum_{\text{angles}} K_\theta(\theta - \theta_{\text{eq}})^2 + \sum_{\text{dihedrals}} \frac{V_n}{2} [1 + \cos(n\phi - \gamma)] + \sum_{\text{nonbonded}} \left[ \frac{C_{ij}}{R_{ij}^{12}} - \frac{D_{ij}}{R_{ij}^6} \right] + E_{\text{electro}} \quad (15)$$

We represent the electrostatic energies in eq 15,  $E_{\text{electro}}$ , by Coulombic ( $A_{ij}$ ) and reaction field terms ( $B_{ij}$ ) of eq 4. The cross Coulombic and reaction field terms together ( $B_{i \neq j}$  and  $A_{i \neq j}$ ) represent pairwise electrostatic energies with an effective dielectric constant, while the self-reaction-field terms ( $B_{i=j}$ ) account for the solvation energies of the protein atoms. In this sense eq 15 stands out from other standard force field energies. In section 3 we have already provided expressions for the bulk solvent contribution to  $\lambda$  through a dielectric continuum model. However, that bulk solvent contribution should not be confused with the electrostatic contribution to solvation energy as incorporated in eq 15 through the reaction field terms. In terms of Figure 3, the protein relaxation and fluctuations occur along the horizontal  $X \leftrightarrow C$  lines. Along this direction the bulk solvent is always in equilibrium and contributes toward equilibrium solvation energies.

Normal mode analysis assumes that the conformational energy  $E$  is harmonic within the range of thermal fluctuations. Thus in terms of the collective NM variables  $\sigma_k$ ,

$$E = \sum_{k=1}^{3(M+N)-6} \frac{1}{2} \omega_k^2 \sigma_k^2 \quad (16)$$

where  $\omega_k$  is the angular frequency of the  $k$ th NM variable. In the sense of principal component analysis,  $\omega_k$  is the effective angular frequency of the  $k$ th principal component variable. This collective variable  $\sigma_k$ , along with the NM basis vectors,  $\alpha_{ik}$ , dictates the displacement of the mass-weighted Cartesian coordinates,  $\Delta X_i$  ( $i = 1, \dots, 3(M+N)$ ), around the MEC by

$$\Delta X_i = \sum_k \alpha_{ik} \sigma_k \quad (17)$$

In normal mode analysis, diagonalization of the hessian matrix,  $\mathbf{F}$  ( $F_{ij} = \partial^2 E / \partial x_i \partial x_j$ ), evaluated at the MEC yields  $\omega_k^2$  as the diagonal elements and  $\alpha_{ik}$  as the  $ik$ th element of the basis set  $\alpha$ . In principal component analysis, diagonalization of the second moment matrix gives corresponding quantities. Each NM variable  $\sigma_k$  therefore defines a collective motion of the protein through eq 17 with a characteristic frequency  $\omega_k$ . The time dependence of  $\sigma_k$  is given by

$$\sigma_k(t) = A_k \cos(\omega_k t + \delta_k) \quad (18)$$

where  $\delta_k$  is the phase and  $A_k$  is the amplitude of the  $k$ th mode. At a given temperature the classical mean-square fluctuation ( $A_k^2/2$ ) of the  $k$ th mode is given by

$$\langle \Delta \sigma_k^2 \rangle_{\text{classical}} = \frac{k_B T}{\omega_k^2} \quad (19)$$

**4.2. Mode-Specific Coupling Coefficient and Reorganization Energy.** The R and the P states in ET reactions are set up

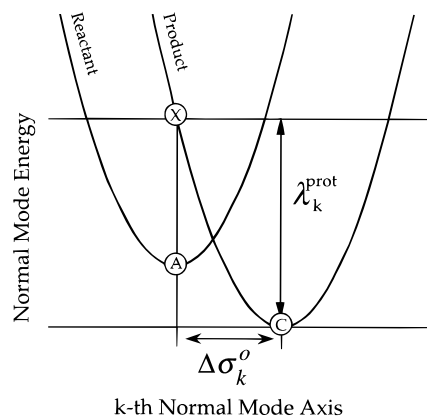


**Figure 4.** Normal mode potential energy before and after ET along the  $k$ th NM axis  $\sigma_k$  (see eq 19).

by the two different charge distributions at the red-ox sites. Correspondingly these two potential energy surfaces (PES) contain two distinct MECs, MEC<sub>R</sub> and MEC<sub>P</sub>. In this respect, the ET problem is different from many other protein conformational studies characterized by a single PES spanning many local MECs. Despite this difference, if the MEC<sub>R</sub> and MEC<sub>P</sub> resemble each other very closely in the conformational space, as experimentally verified for ET proteins,<sup>32,33</sup> only one set of NM vectors will suffice to represent the dynamics around both the MECs. This specific feature of the ET problem is analogous to the situation in the NMA of two distinct MECs on a single PES, although several other features of the ET problem resemble those that are found in molecular spectroscopy.

As shown in Figure 4, the NM energies before and after ET (R and P) can be written as

$$E^R = \frac{1}{2} \sum_k \omega_k^2 \sigma_k^2$$

$$E^P = \frac{1}{2} \sum_k \omega_k^2 (\sigma_k - \Delta \sigma_k^o)^2 - \Delta E^o \quad (20)$$

where  $\Delta \sigma_k^o$  is the NM variable shift of MEC<sub>P</sub> with respect to MEC<sub>R</sub> along the  $k$ th NM variable and  $\Delta E^o$  is the energy difference between the two MECs.

Equation 20 assumes that there is no frequency change associated with the ET process and that the same set of eigenvectors can describe fluctuations around the two MECs before and after ET. Justification for using the same set of NM vectors for the initial and final state comes, besides the structural similarity of reduced and oxidized proteins, from simulation studies which show that the low-frequency modes span the same "important" conformational subspace around MECs that are close to each other in the conformational space.<sup>34</sup> The advantage of using only one set of eigenvectors is that one can construct a concrete reaction coordinate (in the conformational space). As will be shown in Figure 4 of the following paper,<sup>24</sup> the assumption embodied in eq 20 is very well satisfied in the real system.

In analogy with the total  $\lambda$  of Figure 1, one may define a protein reorganization energy  $\lambda^{\text{prot}}$  as the energy associated with the relaxation of only the protein nuclear coordinates as the charge distribution on the red-ox sites changes. Within the NM description this will have components along all the NM axes, and the  $k$ th mode contribution is shown schematically in Figure 4.

From a simple geometric argument, the two parabolas of eq 19 yield the reorganization energy corresponding to the  $k$ th

normal mode as

$$\lambda_k^{\text{prot}} = \frac{1}{2} \omega_k^2 (\Delta\sigma_k^\circ)^2 \quad (21)$$

The total protein reorganization energy  $\lambda^{\text{prot}}$  is given by a sum over all modes as

$$\lambda^{\text{prot}} = \sum_k^{3(M+N)-6} \lambda_k^{\text{prot}} \quad (22)$$

Equations 21 and 22 provide a means to decompose the total protein reorganization energy into a spectrum which comprises contributions from individual modes.

From an inspection of eqs 21 and 22 it is evident that the key quantity that determines either the mode-specific coupling coefficient or the reorganization energy is the horizontal shift along that particular mode  $\Delta\sigma_k^\circ$ . One way to calculate the set of shifts  $\Delta\sigma_k^\circ$  is to perform two sets of NMAs around the conformations MEC<sub>R</sub> and MEC<sub>P</sub>. However, as pointed out earlier, we propose to carry out only one set of NMA and directly determine the shifts  $\Delta\sigma_k^\circ$ . The energy difference between the R and the P states at a given protein conformation can be written as

$$\Delta E(\sigma_k) = E^R - E^P = \left[ \Delta E^\circ - \frac{1}{2} \sum_k \omega_k^2 (\Delta\sigma_k^\circ)^2 \right] + \sum_k (\omega_k^2 \Delta\sigma_k^\circ) \sigma_k \quad (23)$$

An expression for  $\Delta\sigma_k^\circ$  follows from eq 23 as

$$\Delta\sigma_k^\circ = \frac{1}{\omega_k^2} \left\{ \frac{\partial}{\partial \sigma_k} (E^R - E^P) \right\} \quad (24)$$

Even though it is possible to derive an analytic expression of  $\Delta\sigma_k^\circ$  from eq 24 by using an explicit expression of electrostatic energy for the R and P states, it is more practical to calculate  $E^R$  and  $E^P$  numerically for a given values of  $\sigma_k$  and carry out the differentiation of eq 24 numerically. This method is employed in the accompanying paper.<sup>24</sup>

Equation 23 also serves as the definition for the mode-specific e-c coupling coefficient. The energy difference  $\Delta E(\{\sigma_k\})$ , given by a linear combination of the NM variables  $\{\sigma_k\}$ , is a convenient representation of the generalized reaction coordinate for the ET reaction.<sup>17</sup> Thus, the linear coupling coefficients  $c_k$  are given by

$$c_k = \omega_k^2 \Delta\sigma_k^\circ \quad (25)$$

Use of a simple continuum dielectric to represent the bulk solvent through the TK model is an important part our model. Despite the simplifications and assumptions that this representation carries, it has advantages too. Use of the TK reaction field energies allows the model to incorporate ionic strength effects on the mode coupling strengths in a straightforward manner. The analytical form of reaction field energies that we employ in this work contains individual terms (direct and reaction field arising between and among the protein and red-ox site atoms) with clear physical meanings. The simple model used in this work can be extended by packing the spherical cavity with a finite number of solvent molecules.<sup>35</sup>

**4.3. Comparison of NMRES Model with Other Linear Models.** In the present work protein fluctuation is represented by collective NM variables, and the coupling of these collective

modes to ET is brought in through the fluctuations of the energy difference of the initial and final states. This energy difference is approximated by a hyper plane (eq 23) and reduces the theory to the case of "linear coupling".

Many elaborate theories have been developed in solid-state physics based on a linear coupling assumption at the outset, such as the spin-boson (SB) model, an approximation that still leaves a tremendous amount of physically interesting behavior. The SB Hamiltonian, which models the electronic degrees of freedom as a spin (two-state Hamiltonian) coupled to a medium comprising a large number of independent harmonic oscillators (the bosonic bath), is given by

$$H_{\text{SB}} = \begin{pmatrix} E^R & H_{\text{DA}} \\ H_{\text{DA}} & E^P \end{pmatrix} \quad (26)$$

If the bath oscillators are identified with only the protein modes,  $E^R$  and  $E^P$  in eq 26 become identical to  $E^R$  and  $E^P$  defined in eq 20. For this reduced bath (protein only), the Hamiltonian can be elaborated as

$$H_{\text{SB}} = (H_{\text{DA}}) \sigma_x + \left( \frac{\Delta E^\circ}{2} \right) \sigma_z + \left\{ \sum_j \frac{1}{2} \omega_j^2 Y_j^2 \right\} 1 + \left( \frac{1}{2} \sum_j c_j Y_j \right) \sigma_z + \left( \sum_j \frac{1}{8} \omega_j^2 \Delta\sigma_j^{\circ 2} - \frac{\Delta E^\circ}{2} \right) 1 \quad (27)$$

where  $\sigma_z$  and  $\sigma_x$  are Pauli spin matrices. The first two terms in eq 27 represent the electronic part of the Hamiltonian;  $H_{\text{DA}}$  and  $\Delta E^\circ$  have already been defined in eqs 1 and 19, respectively. The third term represents the harmonic bath, where  $Y_j$  are the mass-weighted bath coordinates ( $=\sigma_k - \Delta\sigma_k^\circ/2$ ) and  $\omega_j$  are the corresponding frequencies. The fourth term in eq 27 is part of the Hamiltonian that represents the coupling of ET to the harmonic bath. Each  $j$ th bath mode, with frequency  $\omega_j$ , linearly couples to ET through a coupling coefficient  $c_j$  already introduced in eq 25.

Once the coupling coefficients  $c_j$  are known, one can construct the spectral function  $J(\omega)$

$$J(\omega) = \frac{\pi}{2} \sum_j \frac{c_j^2}{\omega_j} \delta(\omega - \omega_j) \quad (28)$$

A knowledge of the spectral function  $J(\omega)$ , the energy difference  $\Delta E^\circ$ , and the electronic coupling element  $H_{\text{DA}}$  completely determines the dynamics of the system, including ways to determine the rate constants. Various ways to obtain ET rates in the framework of the multimode SB Hamiltonian are discussed extensively by Schulten and co-workers, and we refer the interested reader to their work and references therein.<sup>10-13</sup>

A detailed review on the SB model has been presented by Leggett et al.<sup>36</sup> The idea of employing the SB formalism to ET is not new. Extensive applications of the SB Hamiltonian to study the problem of ET have been done by Onuchic,<sup>37-39</sup> Chandler,<sup>40,41</sup> Schulten,<sup>11-13</sup> and their co-workers. The dispersed polaron approach used by Warshel and co-workers<sup>15</sup> can also be shown to be an approximation of the SB model at high temperatures. Among these approaches, Schulten's work comes closest to what we present here. Schulten, like us, used a multimode Hamiltonian which allows inclusion of contributions arising from all modes. However, there are important differences between the present work and Schulten's. The difference primarily lies in the fact that we use a reduced bath, and more

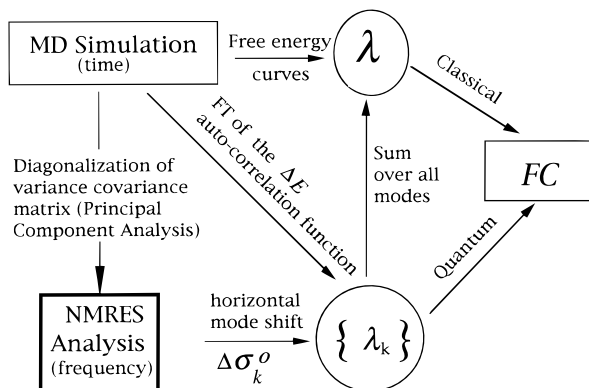


**Figure 5.** Schematic comparison of various treatments of coupling of ET to medium nuclear fluctuations.

importantly, the bath modes are not spatially anonymous in our work: this point is elaborated below.

Another difference is that we treat the system classically. Extension of our treatment to a quantum system can be done, for example, by using the method proposed by Shulten.<sup>11–13</sup>

In Figure 5, we schematically show how our work fits in with other approaches. The starting point of our simulations, the frequency domain, is highlighted for clarity in Figure 5. Unlike the present work, all other models start from an MD simulation in the time domain. This yields free energy curves of Figure 1 through probability distributions of  $\Delta E(\mathbf{r}[t])$ ,<sup>16</sup> or alternatively, the spectral function  $J(\omega)$ , defined by eq 28, can be obtained by the Fourier transform of the  $\Delta E$  autocorrelation function.<sup>11</sup> The latter method makes the bath modes anonymous as far as the associated atomic fluctuations go, which we call “spatial-anonymity”. This spatial-anonymity is different from the following “frequency-anonymity”. As far as the computation of the rate constant goes, the former is totally irrelevant, while the latter is tolerable only for the low-frequency classical modes.

The important characteristic here is that for a given temperature the high-frequency modes must be treated individually, each possessing their individual characteristic frequency  $\omega_k$ , and their individual couplings to the state change at the red-ox site, captured in the reorganization energy parameters  $\lambda_k$ . On the other hand, for modes of sufficiently low frequency, their respective reorganization energies can be summed together and the aggregate coupling described by a single  $\lambda$  ( $\lambda_{\text{out}}$ ) corresponding to a single classical oscillator.

This simplification arises from the irrelevance of the frequency  $\omega_k$  to the thermal excitation of a classical oscillator, hence the frequency-anonymity of the low-frequency classical modes as far as the FC is concerned. When  $J(\omega)$  is obtained by a Fourier transform from the time domain, the modes are assigned a frequency signature. Nevertheless, whether low frequency and not-low frequency, all modes still have individual spatial signatures, useful in the spatial examination of the e–c coupling. This spatial characteristic of the modes is lost unless either an NM analysis is performed as we propose here or the MD simulation data are analyzed by a principal component analysis.<sup>25</sup> Our model enjoys all the advantages that the SB formalism offers, yet it is this inclusion of the spatial signatures of the modes where it stands out from other models that also employ the multimode Hamiltonian model.

As a direct consequence of the spatial information of the bath modes, a series of structural analyses can be performed. For example, given a set of modes that couple most to ET, we can identify parts of the polypeptide chain, the cofactors, or the

bound solvent molecules whose fluctuations are important. It is to be noted that since the fluctuations are modeled to be collective, even long-range spatial couplings will show up.

**4.4. A New Way of Partitioning Total  $\lambda$ .** As a consequence of using a reduced bosonic bath (reduced because it lacks one degree of freedom originating from the solvent) for representing the protein system and treating the bulk solvent contribution separately, we have effectively expressed the total  $\lambda$  as

$$\lambda = \lambda^{\text{blk}} + \sum_k \lambda_k^{\text{prot}} \quad (29)$$

In contrast to this, the usual way to decompose  $\lambda$  is the following:<sup>3</sup>

$$\lambda = \lambda_{\text{in}} + \lambda_{\text{out}} \quad (30)$$

where the solvent contributions make up a single  $\lambda_{\text{out}}$  and the high-frequency skeletal vibrations of the red-ox center make up  $\lambda_{\text{in}}$  through expressions similar to eqs 21 and 22. When applied to ET in ions and small molecules, this is a reasonable breakup.

However, eq 30 becomes unsuitable when  $\lambda$  is estimated for protein ET. Not only the solvent but also the protein matrix contribute significantly to  $\lambda_{\text{out}}$ , as

$$\lambda_{\text{out}} = \lambda_{\text{solvent}} + \lambda_{\text{protein}} \quad (31)$$

Estimation of the total  $\lambda_{\text{out}}$ , as proposed in eq 31, was performed in an earlier work.<sup>18</sup> However, what we propose here (eq 29) is not merely a calculation of the protein and bulk solvent contributions separately, but in our treatment, the protein contribution is explicitly spread over all the collective modes including the high-frequency modes that contribute to  $\lambda_{\text{in}}$ . Because through eqs 21 and 22 we calculate the entire protein  $\lambda$  spectrum,  $\lambda_{\text{in}}$  can be estimated as a sum over all modes above a certain cutoff frequency (say 150  $\text{cm}^{-1}$ ), whereas the remaining low-frequency modes would account for the protein contribution in  $\lambda_{\text{out}}$ .

$$\lambda_{\text{in}} = \sum_{k:\omega_k > 150\text{cm}^{-1}} \lambda_k^{\text{prot}}$$

$$\lambda_{\text{out}} = \sum_{k:\omega_k < 150\text{cm}^{-1}} \lambda_k^{\text{prot}} + \lambda^{\text{blk}} \quad (32)$$

This is a more natural way of analyzing  $\lambda$  in protein ET. Note that since we include self-energies in the NM energies, high-frequency skeletal vibrations of the same red-ox skeleton (heme, for example) will contribute differently to  $\lambda_{\text{in}}$  depending upon whether it is at the core of a protein or it is solvent exposed.

## 5. Summary

Although several theoretical approaches are available to gauge the role of protein medium in controlling ET, in terms of addressing certain questions at the molecular level, such as whether some specific structural fluctuations are essential for controlling ET or not, there was a gap between the existing theories and their applicability to experimental systems. To bridge this gap and in continuation of our efforts to model protein structure and function from a collective motion viewpoint, we have presented a model that quantitatively connects collective protein fluctuation to ET.

Both the bulk solvent and the protein are treated to couple to ET. The bulk solvent is represented by a structureless dielectric

continuum within which the protein molecule is contained in a separate low-dielectric cavity. Protein fluctuations are modeled by collective NM vectors, which include equilibrium solvation effects through reaction field terms. While the coupling of bulk solvent and ET is expressed through a single parameter,  $\lambda^{\text{blk}}$ , the protein component of the coupling is expressed as a spectrum spanning all the NM axes. The primary aim of formulating this model was not to calculate rate constants or provide insights into any new physics, but rather we wanted to assign functional importance to specific NM fluctuations, and this is reflected in the  $\lambda^{\text{prot}}$  spectrum. In our model, the implicit assumption of linear coupling to ET makes it equivalent to a reduced SB formalism where the reduced bosonic bath is represented by the harmonic protein NMs. The SB model has been applied to the problem of ET by others in previous studies. However, there are several new aspects that our work brings out.

Previously Schulten and co-workers had used a multimode Hamiltonian to describe the photosynthetic reaction center. Their starting point, like others, was a molecular dynamics simulation in the time domain which was used to access the spectral function  $J(\omega)$  crucial in determining the ET rate by a Fourier transform of the energy–energy correlation function. Contrary to their work, our starting point is the NM analysis in the frequency domain. This allows our model to structurally identify all the bath modes in  $J(\omega)$ . This is important if one wants to correlate specific structural fluctuations of the protein to ET coupling. Thus our model has all the advantages of a SB model (connection to rate constants) with the added advantage that the individual bath modes are no longer spatially anonymous. The present analysis is not just restricted to harmonic NMs, but instead one can use data from an MD run and through a principal component analysis construct collective modes that represent the bath oscillators.

In the present work since all the protein atoms, including the red-ox sites, were allowed to fluctuate, we did not calculate the total  $\lambda$  as is usually done by calculating its components,  $\lambda_{\text{in}}$  and  $\lambda_{\text{out}}$ . Instead the total  $\lambda$  is a combination of  $\lambda^{\text{prot}}$  and  $\lambda^{\text{blk}}$ . The  $\lambda^{\text{prot}}$  term is a sum of contributions from all the individual protein NMs including ones that contribute to  $\lambda_{\text{in}}$ . The equilibrium solvent contribution to  $\lambda$  gets partitioned onto each mode depending upon how much that particular mode fluctuation, as the charge distribution changes, couples to the solvent outside the cavity. This a more natural way of breaking up the total  $\lambda$  and the first time that a breakup in this manner has been presented. Churg et al.<sup>18</sup> had earlier attempted to resolve the total  $\lambda$  as contributions from the protein and the bulk solvent, but the  $\lambda^{\text{prot}}$  was never resolved into a spectrum as we do here.

Future work will involve improving both our model and its application to systems that have been experimentally studied. There are two obvious ways in which the present model can be extended. The first is by replacing the NM vectors by principal components,<sup>34</sup> and the second is by using a more realistic shape of the protein while calculating the reaction field energies. While the first is straightforward, the latter could be computationally too demanding. One possibility would be to use approximations as was used by Beglov and Roux<sup>35</sup> in calculating reaction field energies. They calculate the configuration-dependent solvation free energy of an effective cluster containing an arbitrarily shaped solute and a finite number of explicit solvent molecules placed inside a hard sphere which is surrounded by a continuum dielectric. To demonstrate the applicability of the present model, we present simulation results on His33-modified cytochrome *c* in an accompanying paper.<sup>24</sup>

Finally, we would like to point out how, as a novel application, the present model can allow analysis of pressure effects on ET rates. Theoretical studies of pressure effects on NMs were studied by Yamato et al.<sup>42</sup> Experiment data of pressure effects on rates of ET exist for cytochrome *c*.<sup>43</sup> Data from this study have been analyzed exclusively by considering the effect of packing (as a function of pressure) on the electronic matrix element  $H_{\text{DA}}$ . With the present model, one can analyze how the reorganization energy  $\lambda$  changes with pressure by combining our model with the work of Yamato et al.<sup>42</sup>

**Acknowledgment.** This work was supported by funds provided by the Ministry of Education and Culture, Japan, the Japanese Society for Promotion of Science (JSPS), and the Human Frontier Science Program Organization (HFSP). A part of the computation was done at computer centers of the Institute for Molecular Science and of the Japan Atomic Energy Research Institute. G.B. was a recipient of PD fellowships from HFSP and JSPS and acknowledges continued support from CSIR, India. We thank Prof. K. Schulten for making a preprint (ref 13) available to G.B.

## References and Notes

- (1) Vervoort, J. *Curr. Opin. Struct. Biol.* **1991**, *1*, 889–894.
- (2) DeVault, D. *Quantum-Mechanical Tunneling in Biological Systems*; Cambridge University Press: London, 1981.
- (3) Marcus, R. A.; Sutin, N. *Biochim. Biophys. Acta* **1985**, *811*, 265–322.
- (4) Marcus, R. A. *J. Chem. Phys.* **1956**, *24*, 966–978.
- (5) Marcus, R. A. *J. Chem. Phys.* **1956**, *24*, 979–989.
- (6) Hopfield, J. J. *Proc. Natl. Acad. Sci. U.S.A.* **1974**, *71*, 3640–3644.
- (7) Dogonadze, R. R.; Kuznetsov, A. M.; Vorotyntsov, M. A. *Phys. Status Solidi B* **1972**, *54*, 425–433.
- (8) Kestner, N. R.; Logan, J.; Jortner, J. *J. Phys. Chem.* **1974**, *78*, 2148–2166.
- (9) Kuki, A. Electron Tunneling Paths in Proteins. In *Long-Range Electron Transfer in Biology*; Palmer, G., Ed.; Springer-Verlag: Berlin, 1991; Vol. 75; pp 49–83.
- (10) Nonella, M.; Schulten, K. *J. Phys. Chem.* **1991**, *95*, 2059–2067.
- (11) Schulten, K.; Tesch, M. *Chem. Phys.* **1991**, *158*, 421–446.
- (12) Xu, D.; Schulten, K. Multi-mode coupling of protein motion to electron transfer in the photosynthetic reaction center: spin-boson theory based on a classical molecular dynamics simulation. In *The Photosynthetic Bacterial Reaction Center II*; Breton, J., Vermeglio, A., Eds.; Plenum Press: New York, 1992; pp 301–312.
- (13) Xu, D.; Schulten, K. *Chem. Phys.* **1994**, *182*, 91–117.
- (14) Zheng, C.; McCammon, J. A.; Wolynes, P. G. *Chem. Phys.* **1991**, *158*, 261–270.
- (15) Warshell, A.; Chu, Z. T.; Parson, W. W. *Science* **1989**, *246*, 112–116.
- (16) Marchi, M.; Gehlen, J. N.; Chandler, D.; Newton, M. *J. Am. Chem. Soc.* **1993**, *115*, 4178–4190.
- (17) Warshell, A.; Parson, W. W. *Annu. Rev. Phys. Chem.* **1991**, *42*, 279–309.
- (18) Churg, A. K.; Weiss, R. M.; Warshel, A.; Takano, T. *J. Phys. Chem.* **1983**, *87*, 1683–1694.
- (19) Noguti, T.; Go, N. *Nature* **1985**, *296*, 776.
- (20) Go, N.; Noguti, T.; Nishiwaka, T. *Proc. Acad. Sci. U.S.A.* **1983**, *80*, 3696–3700.
- (21) Gruschus, J. M.; Kuki, A. *J. Phys. Chem.* **1993**, *97*, 5581–5593.
- (22) Onuchic, J. N.; Beraton, D. N.; Winkler, J. R.; Gray, H. B. *Annu. Rev. Biophys. Biomol. Struct.* **1992**, *21*, 349–377.
- (23) Brunschwig, B. S.; Ehrenson, S.; Sutin, N. *J. Phys. Chem.* **1986**, *90*, 3657–3668.
- (24) Basu, G.; Kitao, A.; Kuki, A.; Go, N. *J. Phys. Chem. B* **1988**, *102*, 2085.
- (25) Kitao, A.; Hirata, H.; Go, N. *Chem. Phys.* **1991**, *158*, 447–472.
- (26) Hayward, S.; Kitao, A.; Hirata, F.; Go, N. *J. Mol. Biol.* **1993**, *234*, 1207–1217.
- (27) Warshel, A.; Levitt, M. *J. Mol. Biol.* **1976**, *103*, 227–249.
- (28) Warshel, A.; Russel, S. T. *Q. Rev. Biophys.* **1984**, *17*, 283–422.
- (29) Sharp, K. A.; Honig, B. *Annu. Rev. Biophys. Biophys. Chem.* **1990**, *19*, 301–332.
- (30) Kirkwood, J. G. *J. Chem. Phys.* **1934**, *2*, 351–361.

- (31) Tanford, C.; Kirkwood, J. G. *J. Am. Chem. Soc.* **1957**, *79*, 5333–5339.
- (32) Berghuis, A. M.; Brayer, G. D. *J. Mol. Biol.* **1992**, *223*, 959–976.
- (33) Takano, T.; Dickerson, R. E. *Proc. Natl. Acad. Sci. U.S.A.* **1980**, *77*, 6371–6375.
- (34) Hayward, S.; Go, N. *Annu. Rev. Phys. Chem.* **1995**, *46*, 223–250.
- (35) Beglov, D.; Roux, B. *J. Phys. Chem.* **1994**, *100*, 9050–9063.
- (36) Leggett, S.; Chakravarty, A. T.; Dorsey, A. P. A.; Fisher, A.; Garg, A.; Zwerger, W. *Rev. Mod. Phys.* **1987**, *59*, 2.
- (37) Garg, A.; Onuchic, J. N.; Ambegaokar, V. *J. Chem. Phys.* **1985**, *83*, 4491–4503.
- (38) Onuchic, J. N.; Beraton, D. N.; Hopfield, J. J. *J. Phys. Chem.* **1986**, *90*, 3707–3721.
- (39) Onuchic, J. N. *J. Chem. Phys.* **1987**, *86*, 3925–3943.
- (40) Bader, J. S.; Kuharski, R. A.; Chandler, D. *J. Chem. Phys.* **1990**, *93*, 230–236.
- (41) Chandler, D. Theory of quantum processes in liquids. In *Liquids, Freezing and Glass Transition*; Hansen, J. P., Levesque, D., Zinn-Justin, J., Eds.; Elsevier: New York, 1991; pp 193–285.
- (42) Yamato, T.; Higo, J.; Seno, Y.; Go, N. *Proteins: Struct. Funct. Genet.* **1993**, *16*, 327–340.